Research Square

Preprints are preliminary reports that have not undergone peer review.
They should not be considered conclusive, used to inform clinical practice,
or referenced by the media as validated information.

Engineering of electrospun PCL/Algal polysaccharide/HKUST-1 nanocomposites for potential biomedical applications

Maryam Haghighi

m.haghighi@alzahra.ac.ir

Alzahra University

Zahra Ezzatpour Ghadim

Alzahra University

Article

Keywords: Nanocomposite, HKUST-1, Polysaccharide, Chlorella, Tetraselmis, Wound dressing

Posted Date: November 6th, 2026

DOI: https://doi.org/10.21203/rs.3.rs-11064201/v1

License: This work is licensed under a Creative Commons Attribution 4.0 International License.
Read Full License

Additional Declarations: No competing interests reported.

Engineering of electrospun PCL/Algal polysaccharide/HKUST-1 nanocomposites for potential biomedical applications

Maryam Haghighi[1]*, Zahra Ezzatpour Ghadim

[1]Department of Physical Chemistry and Nanochemistry, Faculty of Chemistry, Alzahra University, Tehran 19938- 93973, Iran

Abstract

In this study, polycaprolactone (PCL), algal-derived polysaccharides, and HKUST-1 were used to fabricate fibrous nanocomposites via electrospinning as a structural platform for potential biomedical applications. Algal polysaccharides were extracted and purified from *Chlorella* and *Tetraselmis*. HKUST-1 was prepared using a hydrothermal method, with $Cu(NO_3)_2 \cdot 3H_2O$ and $Cu(CH_3COO)_2 \cdot H_2O$ as copper precursors. HKUST-1, showed a uniform polyhedral morphology and average particle diameters of approximately 45-50 nm. BET analysis showed mesoporous structures with surface areas of 59.74 and 141.66 m^2/g for the nitrate- and acetate-derived MOFs, respectively. PCL solutions with concentrations of 10, 15, 20, and 35% (w/v) were prepared, along with HKUST-1/PCL solutions containing 0.5, 1, 3, 4, and 5 wt% HKUST-1 relative to PCL. To fabricate the nanocomposites, the PCL solutions were initially electrospun to form the fibrous substrate. The three-layer PCL/algal polysaccharide/HKUST-1 nanocomposites were subsequently fabricated by adding the algal polysaccharide of *Chlorella and Tetraselmis* and HKUST-1 onto the PCL nanofibers. The average fiber diameters ranged from 70–1000 nm. Key fabrication parameters, including solvent type and ratio, solution concentration, and electrospinning conditions, were optimized to obtain uniform and homogeneous nanofibrous structure. The results indicated that the synthesized nanofibers exhibited nanoscale dimensions and a uniform morphology. Incorporating of polysaccharides into the PCL nanofibers increased the surface contact angle from 118° to 130–134°, indicating enhanced surface hydrophobicity. This increase was attributed to the compact molecular structure of the polysaccharides and their limited exposure at the fiber surface during electrospinning. Antibacterial tests revealed that HKUST-1 exhibited antibacterial activity against both *E. coli* and *S. aureus,* with minimum inhibitory concentration (MIC) and minimum bactericidal concentration (MBC) values of 3.75 and 7.5 mg/mL, respectively. The *Tetraselmis*-derived polysaccharide exhibited bacteriostatic

[1] Corresponding Author, Email: m.haghighi@alzahra.ac.ir

activity against *S. aureus*, with an MIC of 25 mg/mL. None of the tested samples exhibited detectable DPPH radical-scavenging activity, which may have been obscured by color interference from the samples at high concentration. This work presents the single-platform nanocomposites combining PCL, *Chlorella*- and *Tetraselmis*-derived polysaccharides, and HKUST-1 MOFs.

Keywords: Nanocomposite, HKUST-1, Polysaccharide, *Chlorella*, *Tetraselmis*, Wound dressing

1. Introduction

Skin, the first line of defense against various external pathogens, is an important part of the immune system in the body. The external skin tissue is damaged due to burns, cuts, and pathological wounds, and on the other hand, the process of wound repair in complex [1-3]. When harmful microorganisms damage the skin surface, they cause infection and inflammation, which results in delayed wound healing. Therefore, advanced wound dressings need to be developed to protect the wound area from infection, contamination, and harmful external factors [4, 5]. The ideal wound dressing for proper protection should have characteristics like moisture retention, water vapor and oxygen permeability, non-toxicity, non-allergenicity, high biocompatibility, and favorable mechanical properties [6, 7]. Nowadays, polymer-based wound dressings synthesized by electrospinning have attracted much attention. Electrospinning is one of the common methods for fabricating nanofibers that use natural and synthetic polymer solutions for this purpose [8]. These fibers are characterized by high porosity, large specific surface area and a high degree of similarity to the human body's natural extracellular matrix [9]. Electrospun nanofibrous dressings are able to absorb wound exudate and efficiently block the external environment, therefore promoting wound healing [10, 11].

Natural polymers, like polysaccharides-including algal polysaccharides-and proteins, when synthetized into nanofibrous dressings, improve wound healing due to their antibacterial and hemostatic properties. These dressings are biocompatible, degradable, and promote cell growth but lack mechanical strength [12-15]. Algal polysaccharides play an important role in wound healing by having antioxidant, anti-inflammatory and antimicrobial properties that are very effective for the wound healing process. These polysaccharides provide suitable conditions for faster healing and can stimulate the growth of new cells by creating a moist matrix at the wound site [16-19]. *Chlorella* and

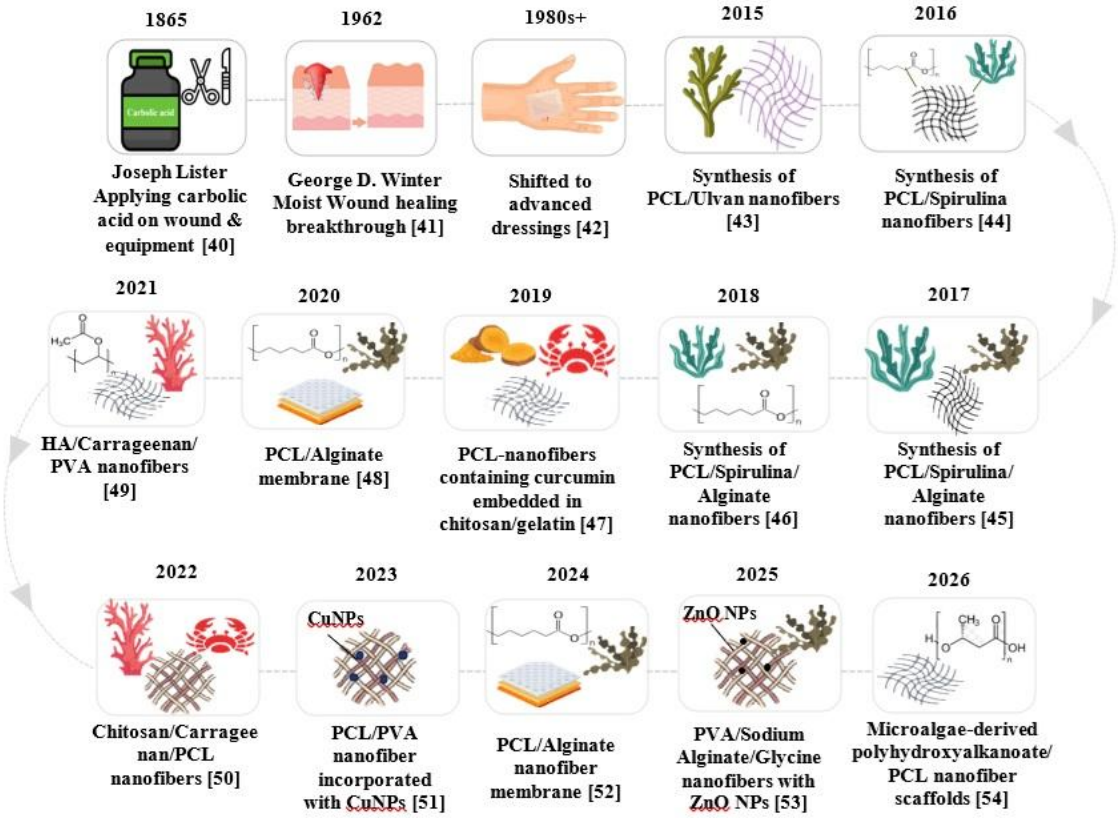
Tetraselmis, two types of green algae, as sources of algal polysaccharides, improve the wound healing process by having biocompatibility, biodegradability, antioxidant and anti-inflammatory properties that help control the secretion of reactive oxygen species and the release of antibacterial products [20-23]. Polysaccharides of *Tetraselmis* can also induce angiogenesis, increase macrophage infiltration, and express TGFβ, which is very effective in accelerating the wound healing process [24].

Synthetic polymers are characterized by high mechanical strength and flexibility in processing but they lack in wound healing efficacy because of relatively low biodegradability and lack of cellular binding sites [25, 26]. Polycaprolactone (PCL) a synthetic polymer, was first synthesized in the early 1930s, drawn much attention due to biodegradability, cell growth stimulation, and viscoelastic properties but was not widely used due to its slow degradation rate [27, 28]. Furthermore, electrospun PCL nanofibers with core-shell structures have been studied for drug delivery, controlled drug release, and wound dressings [29, 30].

Although both natural and synthetic polymers possess multiple excellent properties, their ability to promote wound healing is restricted [31, 32]. To address this, polymeric nanofibrous materials have been utilized as scaffolds for wound dressings, incorporated with therapeutic agents, enabling them to fulfill their roles during different stages of wound healing and improving wound repair outcomes [33]. Electrospun nanofiber dressings loaded with drugs or antibacterial substances, such as metal-organic frameworks (MOFs), indicate improved skin tissue repair and facilitating wound healing [34]. Metal-organic frameworks have high specific surface area, easy surface modification and tunable pore size, which make them suitable for drug loading, transport, and controlled release. Some studies have shown the antibacterial properties of copper-based metal-organic frameworks (such as Cu-MOF-74 and HKUST-1) which are the result of gradual copper ion release. The metal centers are slowly and gradually released as a result of the degradation of the metal-organic framework [35-38]. The instability of metal-organic frameworks in physiological solutions greatly limits their direct use in wound healing, and therefore, to exploit the properties of these materials, they should be loaded onto polymer substrates, including nanofibers [39].

A summary of studies investigating the use of nanofibers loaded with natural polymers such as algal-derived polymers, and nanoparticles for tissue regeneration and wound healing is described in detail subsequently (Scheme. 1). The development of wound dressing focused primarily on infection control and progressed to the design of bioactive

systems to accelerate tissue repair. This process began in 1865 with the use of carbolic acid (phenol) by Joseph Lister for the disinfection of wounds, dressings, and surgical equipment, and brought about a major revolution in the prevention of surgical infections [40]. In 1962, George D. Winter established the scientific basis for advanced wound dressings by demonstrating that wounds heal up to 50% faster in a moist environment than in a dry environment [41]. Based on this finding, from the 1980s, traditional dry dressings gradually gave way to advanced dressings with the ability to retain moisture and stimulate tissue regeneration. With the advancement of electrospinning technology, research was directed towards the development of bioactive nanofibers based on synthetic and natural polymers [42]. In 2015, the PCL/Ulvan nanofibrous biocomposites were synthesized as an advanced wound dressing [43]. Subsequently, nanofibers incorporating *Spirulina* extract as well as *Spirulina*-alginate/PCL were developed to increase antioxidant properties, retain moisture, and accelerate tissue regeneration [44, 45]. In 2018, dressings with suitable antimicrobial and biocompatible properties were produced by adding quaternary ammonium salts to PCL/gelatin nanofibers [46].



Scheme. 1. Key studies investigating the use of algae in healing applications

The use of biopolymers and polysaccharides such as collagen, starch and alginate along with polycaprolactone and polyvinyl alcohol (PVA), led to the development of nanofibers with favorable mechanical and regenerative properties [47-51]. In recent years, research has focused on the loading of different nanoparticles, such as copper and zinc oxide nanoparticles onto the nanofibers, along with incorporating of stem cells and microalgae into fibrous nanocomposites [52-54]. To the best of our knowledge, the fabrication and structural characterization of electrospun nanofibers incorporating polycaprolactone, algal polysaccharides derived from *Tetraselmis* and *Chlorella*, and HKUST-1 have not yet been reported. The main goal of this study was to fabricate algal polysaccharide-based nanofibers with an optimized structural configuration. PCL was incorporated as a co-polymer because the algal polysaccharide alone is incapable of electrospinning. In addition, PCL was employed to further enhance the physicochemical properties of the resulting nanofibers. The fabricated nanofibers were subsequently loaded with HKUST-1 to import the desired functional properties.

2. Experimental work

2. 1. Materials

Polycaprolactone (Mw=80000 $g \cdot mol^{-1}$), $Cu(NO_3)_2 \cdot 3H_2O$, $Cu(CH_3COO)_2$, 1,3,5-benzenetricarboxylic acid (H_3BTC) were purchased from Sigma-Aldrich Reagent Co. Ltd (Steinheim, Germany). The solvents including formic acid, glacial acetic acid, and N,N-dimethylformamide (DMF) were sourced from Merck (Darmstadt, Germany). Absolute ethanol was prepared from Ghatran Shimi Co. (Ghazvin, Iran). Double distilled water was applied in all experiments. In this study, the dried powder of green microalgae was used for the preparation of the composites. *Chlorella* and *Tetraselmis* were prepared from Iranian company Qeshm Micro Algae Biorefinery (QMAB). All chemicals were of analytical grade and used without further purification.

2. 2. Instruments

Firstly, the samples were observed by optical microscope model Nikon eclipse E100 (Nikon Corporation, Tokyo, Japan). Fourier transform infrared (FTIR) and attenuated total reflection (ATR) spectra were recorded by a *Bruker, tensor 27* spectrometer (Bruker Optik GmbH, Ettlingen, Germany). The morphologies of the prepared samples were studied by scanning electron microscope (SEM) model TESCAN VEGA3 (Brno, Czech Republic). The BET analyzer model TriStar II 3020 (Micrometrics Instrument

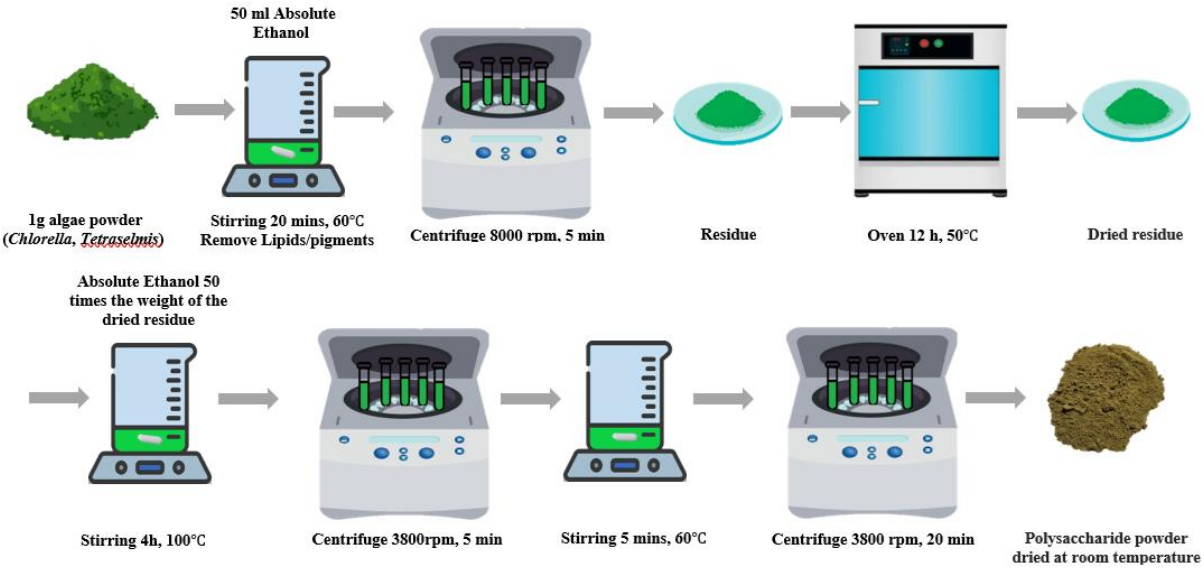
Corporation, Georgia, USA) was applied to study the surface area and porosity of the samples. Jikan-CAG 20 SE device (Jikan Surface Nano-Engineering Co., Tehran, Iran) was applied to measure the contact angle of water droplets with surface of the samples. The electrospinning machine model Full Option Lab2 ESI-II (Fanavaran Equipment Nanoazma Co., Tehran, Iran) was used in this study.

2. 3. Synthesis of HKUST-1

In this study, HKUST-1 was synthesized according to the reported method in references [55, 56] with some modifications. Briefly, 0.071 g of $Cu(NO_3)_2 \cdot 3H_2O$ was dissolved in a mixture of 10 mL of double distilled water and 8 mL of absolute ethanol. Furthermore, 0.043 g H_3BTC was dissolved in the similar solvent mixture with equal volumes (10 mL of double distilled water and 8 mL of absolute ethanol). In continuation, the copper solution was added dropwise to the H_3BTC solution under continuous stirring. The resulting mixture was transferred into a teflon-lined stainless-steel autoclave and then was placed in an oven at 120 ℃ for 24 h to form the blue crystals. Subsequently, the synthesis was performed using 0.071 g $Cu(CH_3COO)_2$ that was dissolved in a solvent mixture consisting of 8 mL of double distilled water and 10 mL N,N-dimethylformamide. Meanwhile, 0.043 g H_3BTC was dissolved in the similar solvent mixture of double distilled water and DMF in equal volumes. The synthesis was followed in the same way as before and a blue precipitate was obtained.

2. 4. Extraction of algal polysaccharides

Polysaccharides were extracted from two different green algae species, *Chlorella* and *Tetraselmis*, according to a two-step extraction method reported in previous studies [57, 58] with slight modifications. In brief, 50 mL absolute ethanol was added to 1 g of algal dried powder with mild boiling to remove lipids, pigments and other impurities with low molecular weight and was stirred for 20 min at 60 ℃. The mixture was centrifuged at 8000 rpm for 5 min, and the residue was collected and dried at 50 ℃ for 12 h. In the next step, absolute ethanol was added to the obtained residue (with a precipitate to absolute ethanol ratio of 1:50 (w/v)) and the extraction was proceeded at 100 ℃ for 4 h. The obtained mixture was centrifuged at 3800 rpm for 5 min and the extracted solution was concentrated by heating at 60 ℃ to evaporate the excess ethanol. The polysaccharide precipitate was washed three times with absolute ethanol, and then dried at room temperature (Scheme. 2).



Scheme. 2. Schematic illustration of the extraction of algal polysaccharides

2. 5. Fabrication of PCL fibers (PF_1 to PF_6)

Specific amount of PCL was dissolved in a solvent mixture of acetic acid and formic acid with different ratios according to the reported method with some modifications in reference [59]. The mixture was subjected to vigorous stirring at 3 h to prepare a uniform PCL solution. Then the solution was introduced into a 5 mL syringe with a needle of internal diameter of 0.2 mm for electrospinning. The specifications of the PCL precursor solution and the corresponding electrospinning conditions are presented in Table 1. Among the formulation evaluated, the 20% (w/v) PCL solution prepared in a solvent mixture of acetic acid and formic acid at a 9:1 (v:v) ratio exhibited the most favorable electrospinning performance and was therefore selected as the optimal formulation (PF_1). For the optimum formulation, the flow rate was adjusted at 0.5 mL/h, and the applied voltage was set to 10 kV. The tip-to-collector distance and drum collector of rotation speed were fixed at 16.5 cm and 150 rpm, respectively.

Table 1. Electrospinning conditions for PCL fibers prepared at various concentrations

Sample Name	PCL solution (w/v) %	Acetic acid to formic acid ratio (v:v)	Electrospinning conditions	Optical microscope image of the sample with 4× magnification
PF_1*	20	9:1	Voltage: 10 kV Flow rate: 0.5 mL/h Rotation speed of drum collector: 150 rpm Tip-to-collector distance: 16.5 cm	
PF_2	20	3:7	Voltage: 20 kV Flow rate: 0.5 mL/h	

Sample Name	PCL solution (w/v) %	Acetic acid to formic acid ratio (v:v)	Electrospinning conditions	Optical microscope image of the sample with 4× magnification
			Rotation speed of drum collector: 200 rpm Tip-to-collector distance: 16.5 cm	
PF_3	15	3:7	Voltage: 15 kV Flow rate: 0.5 mL/h Rotation speed of drum collector: 150 rpm Tip-to-collector distance: 16.5 cm	
PF_4	35	3:7	Voltage: 11 kV Flow rate: 0.5 mL/h Rotation speed of drum collector: 150 rpm Tip-to-collector distance: 16.5 cm	
PF_5	15	9:1	Voltage: 8 Kv Flow rate: 0.2 mL/h Rotation speed of drum collector: 150 rpm Tip-to-collector distance: 16.5 cm	
PF_6	10	9:1	Voltage: 8.5 kV Flow rate: 0.2 mL/h Rotation speed of drum collector: 150 rpm Tip-to-collector distance: 16.5 cm	

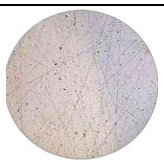
*PF_1 was selected as the optimal sample among the fabricated fibers due to its homogenous morphology

2. 6. Fabrication of PCL fibers loaded with HKUST-1 (NF_1-Cu to NF_7-Cu)

0.2 g of PCL was dissolved in 1 mL of an acetic acid/formic acid solvent mixture at a 9:1 (v:v) ratio under vigorous stirring for 2 h to prepare a 20% (w/v) PCL solution. Then, a specific amount of synthesized HKUST-1 was added to the PCL solution and the mixture was vigorously stirred for 1 h. Then the solution was introduced into a 5 mL syringe with a needle of internal diameter of 0.2 mm for electrospinning. In order to achieve a uniform distribution of HKUST-1 on the fibers, a number of solutions were homogenized under ultrasonication. According to the results summarized in Table 2, a HKUST-1 to PCL ratio of 4% (w/w) was identified as the optimum sample (NF_1-Cu).

Table 2. Electrospinning conditions for PCL fibers containing HKUST-1 at various concentrations

Sample name	HKUST-1 to PCL ratio (w/w) %	Ultrasonic for HKUST-1 distribution in solvent	Electrospinning conditions	Optical microscope image of the sample with 4× magnification
NF_1-Cu*	4	☒	Voltage: 8.5 kV Flow rate: 0.1 mL/h Rotation speed of drum collector: 100 rpm Tip-to-collector distance: 15 cm	
				

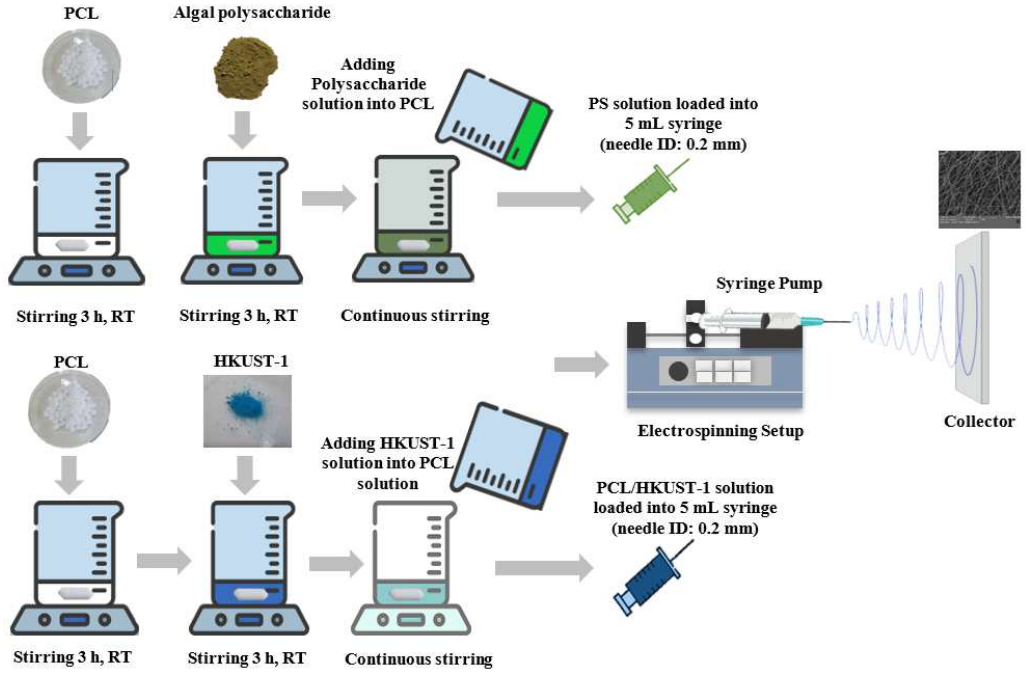
Sample name	HKUST-1 to PCL ratio (w/w) %	Ultrasonic for HKUST-1 distribution in solvent	Electrospinning conditions	Optical microscope image of the sample with 4× magnification
NF_2-Cu	5	☒	Voltage: 8.5 kV Flow rate: 0.1 mL/h Rotation speed of drum collector: 150 rpm Tip-to-collector distance: 16.5 cm	
NF_3-Cu	1	☒	Voltage: 8-10 kV Flow rate: 0.1 mL/h Rotation speed of drum collector: 150 rpm Tip-to-collector distance: 15 cm	
NF_4-Cu	0.5	☒	Voltage: 8.1-10 kV Flow rate: 0.2 mL/h Rotation speed of drum collector: 150 rpm Tip-to-collector distance: 15 cm	
NF_5-Cu	0.5	☑	Voltage: 10 kV Flow rate: 0.1 mL/h Rotation speed of drum collector: 150 rpm Tip-to-collector distance: 15 cm	
NF_6-Cu	3	☑	Voltage: 9 kV Flow rate: 0.2 mL/h Rotation speed of drum collector: 150 rpm Tip-to-collector distance: 15 cm	
NF_7-Cu	4	☑	Voltage: 7-8 kV Flow rate: 0.1 mL/h Rotation speed of drum collector: 150 rpm Tip-to-collector distance: 15 cm	

*NF_1-Cu was selected as the optimal sample among the fabricated fibers due to its homogenous morphology

2. 7. Fabrication of PCL/Algal polysaccharide/HKUST-1 nanocomposites (TNC-Cu, ChNC-Cu, ChNF, and TNF)

PCL and the extracted polysaccharide were separately dissolved in a solvent mixture of acetic acid and formic acid at a 9:1 (v:v) ratio under vigorous stirring for 3 h. The polysaccharide solution was then gradually added to the PCL solution under continuous stirring to prepare the electrospinning precursor solution for the base layer of the nanocomposite. In continuation, specific amounts of PCL and HKUST-1 were separately dispersed in the aforementioned acidic solvent mixture. The HKUST-1 dispersion was then slowly added to the PCL solution under continuous stirring for 3 h. The final solutions were introduced into 5 mL syringes with a needle of internal diameter of 0.2 mm for electrospinning. The flow rate was adjusted to 0.5 mL/h, the applied voltage was

set at 10 kV, and the tip-to-collector distance and drum collector rotational speed were fixed at 12 cm and 100 rpm, respectively. The PCL/polysaccharide solution was initially electrospun to form the base layer of the composite, followed by electrospinning of the PCL/HKUST-1 solution onto the preformed layer (Scheme. 3).



Scheme. 3. Schematic illustration of the electrospinning process for PCL/Algal polysaccharide/HKUST-1 nanocomposite

In order to achieve the optimum sample, different PCL/polysaccharide solutions were prepared and evaluated, and the corresponding results are summarized in Table 3.

Table 3. Electrospinning conditions for nanocomposites

Nanocomposite name	Compositions	Electrospinning conditions
TNC-Cu* (T=*Tetraselmis*)	PCL/*Tetraselmis* polysaccharide/HKUST-1	Voltage: 10 kV Flow rate: 0.5 mL/h Rotation speed of drum collector: 100 rpm Tip-to-collector distance: 12 cm
ChNC-Cu (Ch=*Chlorella*	PCL/*Chlorella* polysaccharide/HKUST-1	Voltage: 10 kV Flow rate: 0.2 mL/h Rotation speed of drum collector: 100 rpm Tip-to-collector distance: 12 cm
ChNF	PCL/*Chlorella* polysaccharide	Voltage: 9 kV Flow rate: 0.2 mL/h Rotation speed of drum collector: 100 rpm Tip-to-collector distance: 15 cm
TNF	PCL/*Tetraselmis* polysaccharide	Voltage: 10 kV Flow rate: 0.7 mL/h Rotation speed of drum collector: 100 rpm Tip-to-collector distance: 15 cm

*TNC-Cu was selected as the optimal sample among the fabricated fibers due to its homogenous morphology

3. Results and discussions

3.1 Characterization of HKUST-1

3.1.1 FTIR spectra of HKUST-1

HKUST-1 MOFs were synthesized in this research using $Cu(NO_3)_2 \cdot 3H_2O$ and $Cu(CH_3COO)_2.H_2O$ and the chemical structures of them were investigated by FTIR spectra in the range of 400-4500 cm^{-1}, that can be seen in Figs. 1a & 1b.

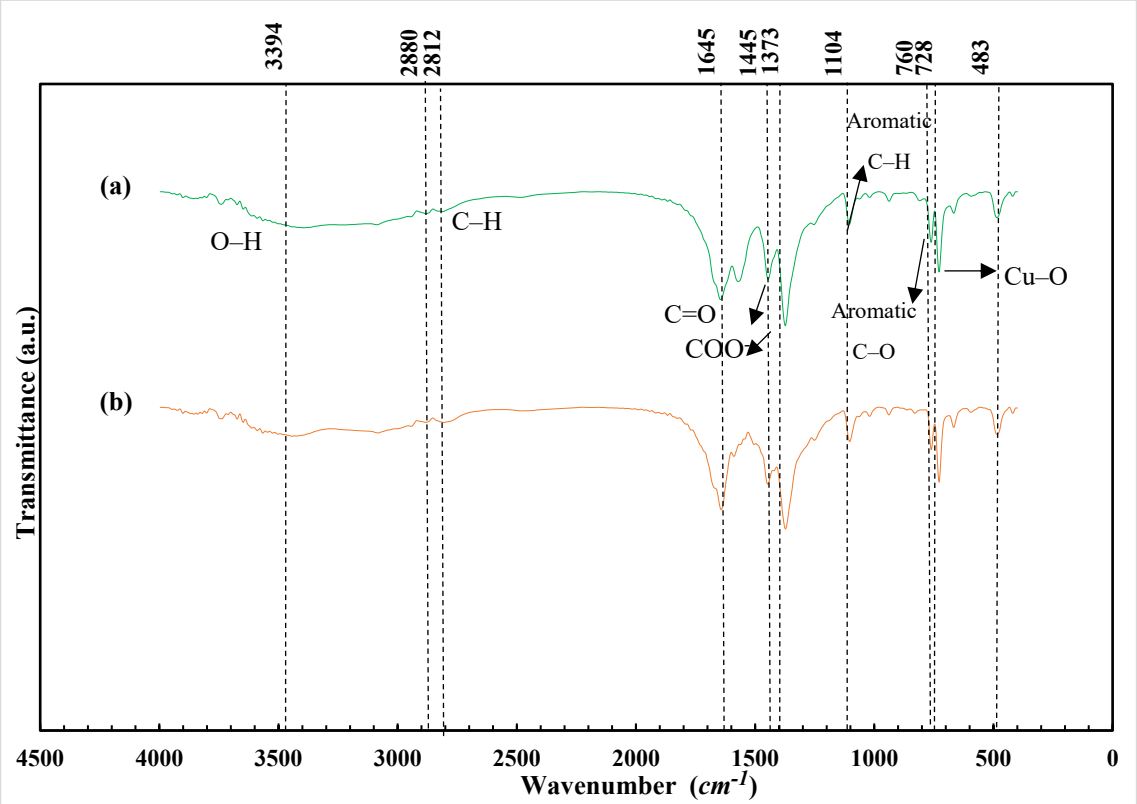


Fig. 1. FTIR spectra of HKUST-1 MOFs **(a)** synthesized with $Cu(CH_3COO)_2.H_2O$, and **(b)** synthesized with $Cu(NO_3)_2.3H_2O$

For both samples, a broad absorption band observed at 3394 cm^{-1} is attributed to the stretching vibrations, which may be due to adsorbed residual water molecules in the structure. The peaks at 2880 and 2812 cm^{-1} are associated with stretching vibrations of C-H and the stretching vibrations of the carbonyl (C=O) group appeared at 1645 cm^{-1}. The peaks observed at 1373 and 1445 cm^{-1} correspond to the stretching vibrations of the carboxylate (COO^-) of the ligand. The peaks at 1104 and 760 cm^{-1} are the result of aromatic C-H and C-O in-plane bending vibrations, respectively [60, 61]. The band at 728 cm^{-1} represented Cu-O stretching vibrations, suggesting the coordination between Cu cations and carboxylic oxygen atoms of BTC ligand [60, 62].

3.1.2 XRD pattern of the synthesized HKUST-1

The XRD patterns of syntheisized HKUST-1 MOFs were presented in Figs. 2a & 2b. The results show, that the X-ray diffraction patterns of HKUST-1 MOFs which were synthesized using $Cu(NO_3)_2.3H_2O$ and $Cu(CH_3COO)_2.H_2O$ are identical. The prominent peaks were appeared at $2\boldsymbol{\theta}$ of 6.7, 9.6, 11.6, 13.5, 17.5, 19, 25.3, 29.3, 30.5, 35, 40, 43.1, and 46.2°. The XRD patterns are in accordance with reported pattern in previous refrences [63], confirming effective synthesis of both prepared samples. In continuation, the crystallinity of the samples was calculated with Origin 2022 software. The crystallinity of synthesized HKUST-1 prepared using of copper acetate was estimated as 60%, while the crystallinity of HKUST-1 synthesized by copper nitrate was calculated about 26%.

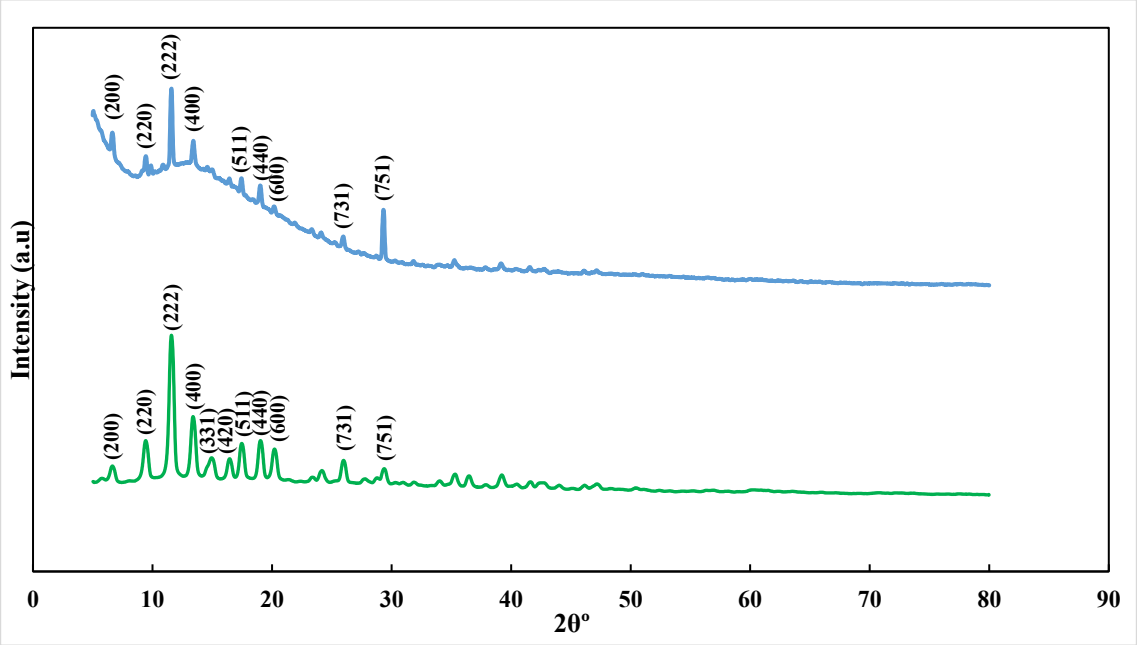


Fig. 2. XRD pattern of HKUST-1 **(a)** prepared by $Cu(NO_3)_2.3H_2O$ and **(b)** prepared by $Cu(CH_3COO)_2.H_2O$

3.1.3 BET analysis of the synthesized HKUST-1

The Brunauer-Emmett-Teller (BET) analysis, is a typical method for determining the specific surface area and porosity of porous samples. This technique relies on the adsorption of gases onto the sample surface at low temperatures. The results of BET analysis of HKUST-1 MOFs were displayed in Figs. 3(a-d). As can be seen in Figs. 3a & 3b, the N_2 adsorption-desorption isotherms of the HKUST-1 are of type IV, which was emphasized the mesoporous structure of the samples (with a pore size of 2 to 50 nm). At high relative pressures, a hysteresis loop was observed, indicating the presence of mesopores. This hysteresis loop is generally attributed to condensation within the pores.

According to the Figs. 3c & 3d, which present the BET surface area measurements, the linearity of the initial portion of the adsorption isotherm at low relative pressure suggests the occurrence of single-layer adsorption. The deviation from linearity at higher relative pressures indicates the onset of multilayer adsorption. The BET surface areas and average pore diameters of HKUST-1 synthesized using of copper acetate and copper nitrate were determined to be 141.6569 m^2/g, 45 Å, and 59.74 m^2/g, 52.63 Å respectively.

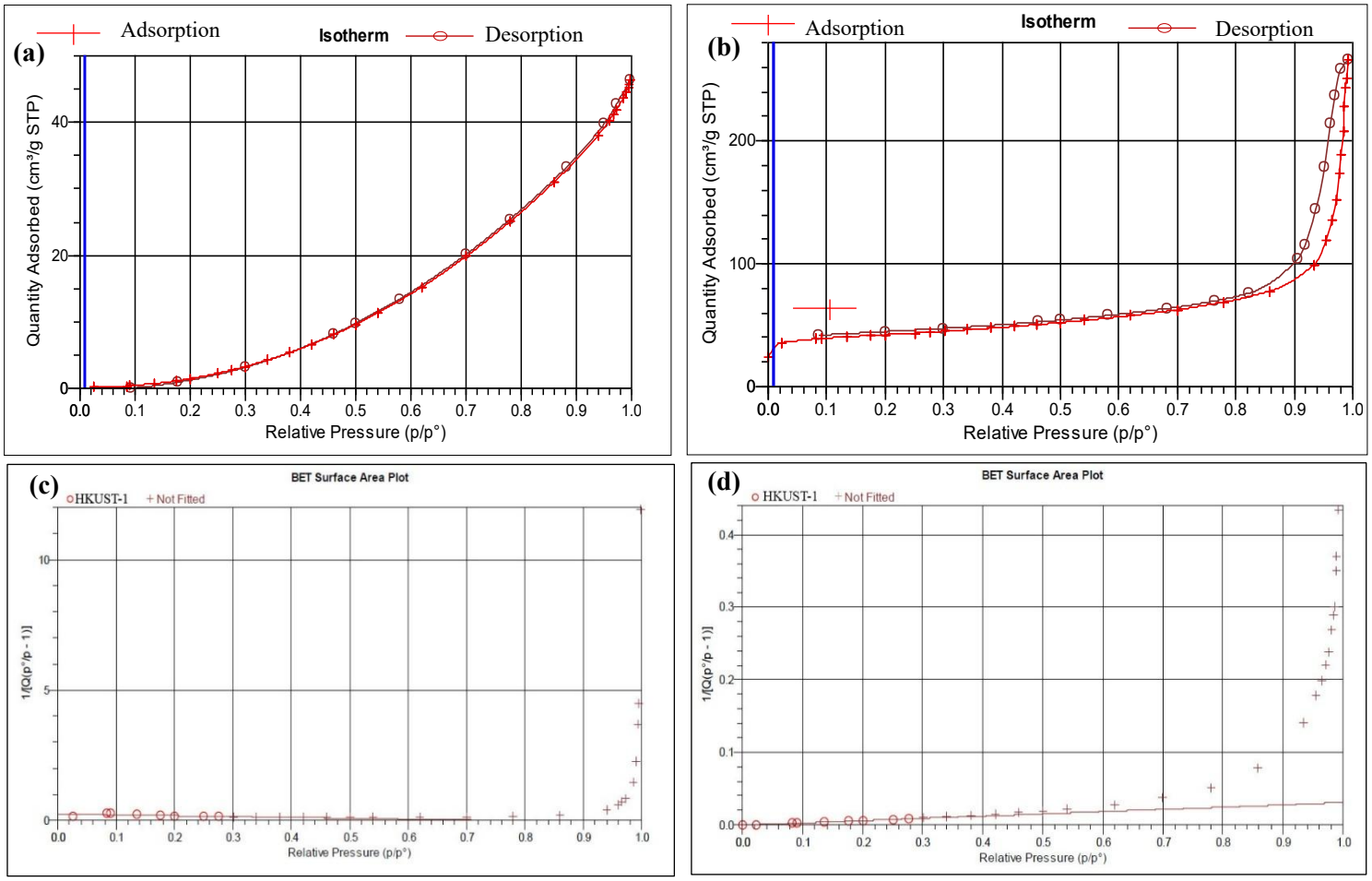


Fig. 3. N_2 adsorption-desorption isotherms of HKUST-1 **(a)** prepared by $Cu(NO_3)_2.3H_2O$, **(b)** prepared by $Cu(CH_3COO)_2.H_2O$, BET surface area plots of HKUST-1 **(c)** prepared by $Cu(NO_3)_2.3H_2O$, and **(d)** $Cu(CH_3COO)_2.H_2O$

3.1.4 SEM images and particle size distribution of HKUST-1 MOFs

The SEM images, Gaussian size distributions, and corresponding average particle sizes of HKUST-1 synthesized using $Cu(NO_3)_2.3H_2O$ as the precursor are presented in Figs. 4(a-d). It can be seen, HKUST-1 have a layered structure with a relatively smooth surface. Using Image J and Origin 2022 software, the average particle diameter of HKUST-1 was estimated to be approximately 47 nm, indicating that the synthesized MOFs are within

the nanoscale range. SEM images and particle size distributions of HKUST-1 synthesized by $Cu(CH_3COO)_2.H_2O$, are displayed in Figs. 4(e-h). The results show that, polyhedral nanoparticles with a crystalline structure, with a smooth surface and homogeneous morphology were formed similar to the reference samples [64]. The average size of the aforementioned HKUST-1, indicate a mean diameter of 45 nm, confirming the nanoscale dimension of the MOFs. As a result, the HKUST-1 synthesized using of $Cu(OAc)_2.H_2O$ has more uniform crystal structure compared to the sample prepared with $Cu(NO_3)_2.3H_2O$.

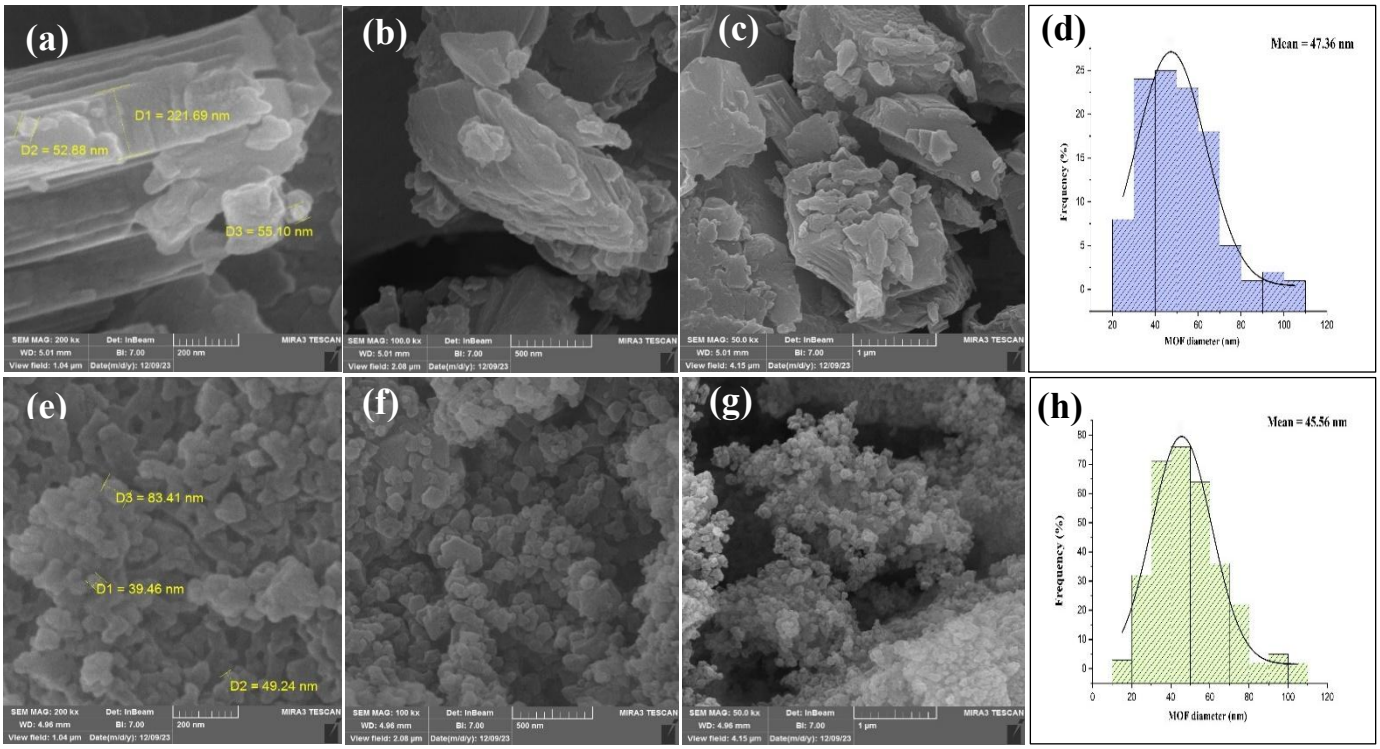


Fig. 4. SEM images and Gaussian size distributions and average particle sizes of HKUST-1 **(a-d)** synthesized by $Cu(NO_3)_2.3H_2O$, and **(e-h)** synthesized by $Cu(CH_3COO)_2.H_2O$

3.2 Characterization of PCL fibers (PF_1), PCL nanofibers containing HKUST-1 (NF_1-Cu), PCL/*Chlorella* polysaccharide nanofibers (ChNF), PCL/*Chlorella* polysaccharide/HKUST-1 nanocomposite (ChNC-Cu), and PCL/*Tetraselmis* polysaccharide/HKUST-1 nanocomposite (TNC-Cu)

3.2.1 FTIR–ATR spectra

The attenuated total reflectance (ATR) mode of Fourier transform infrared spectroscopy is an advanced spectroscopic method used for the identification and analysis of materials at the molecular scale. This technique integrates infrared spectroscopy with attenuated total reflectance, making it appropriate for the analysis of solid, liquid, and semi-solid materials. FTIR-ATR spectroscopy was used to determine the chemical structure of the

prepared samples including PCL fibers containing HKUST-1 (NF_1-Cu), PCL/*Tetraselmis* polysaccharide/HKUST-1 nanocomposite (TNC-Cu), and PCL/*Chlorella* polysaccharide/HKUST-1 nanocomposite (ChNC-Cu), as shown in Figs. 5(a-c). The observed peaks in the range of 2860 and 2940 cm^{-1}, illustrate the symmetric and asymmetric stretching vibrations of the C-H bond. The peak in the range of 1720-1730 cm^{-1} refers to the stretching vibrations of the carbonyl (C=O) group of polycaprolactone. Additionally, the broad peak in the region of 3200-3600 cm^{-1} indicates the stretching vibrations of the hydroxyl group, while the 1600-1650 cm^{-1} peak assigns to the carbonyl group in polysaccharides. Also, a peak at around 728 cm^{-1} relates to the stretching vibrations of Cu-O in HKUST-1.

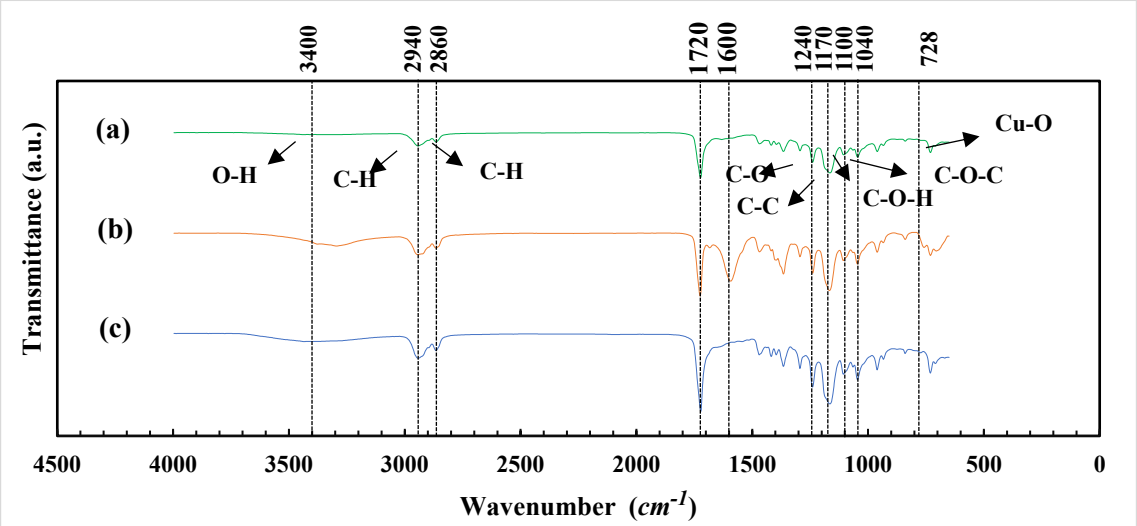


Fig. 5. FTIR-ATR spectra of prepared samples **(a)** PCL fibers containing HKUST-1 (NF1-Cu), **(b)** PCL/*Tetraselmis* polysaccharide/HKUST-1 nanocomposite (TNC-Cu), and **(c)** PCL/*Chlorella* polysaccharide/HKUST-1 nanocomposite (ChNC-Cu)

3.2.2 Surface morphology, size distribution, and SEM-EDS elemental mapping

The SEM image and Gaussian-fitted fiber diameter distribution of the prepared PCL fibers (PF_1) are presented in Fig. 6a. It can be seen in Fig. 6a, the PCL fibers exhibit a well-aligned, bead-free, and interconnected morphology. The Gaussian distributions and average fiber diameter were estimated by ImageJ and Origin 2022 software. Following the aforementioned analytical approach, the average fiber diameter of PF_1 was estimated to be approximately 1300 nm, as shown in Fig. 6a. The morphology of the PCL nanofibers containing HKUST-1 (NF_1-Cu) was characterized by SEM, as shown in Fig. 6b. The nanofibers exhibited a well-aligned and smooth morphology, with HKUST-1 nanoparticles uniformly distributed throughout the nanofibrous matrix. Notabely, the incorporation of HKUST-1 did not result in the formation of beads or other apparent

morphological defects. The results indicate that the incorporation of 4 wt% of HKUST-1 into the PCL solution led to a pronounced reduction in the average diametere of the electrospun fibers (NF_1-Cu), which decreased to 87.12 nm. As shown in the SEM-EDS elemental mapping image of the PCL nanofibers containing HKUST-1 (NF_1-Cu) (Fig. 6c), the elements C, O and Cu were uniformly distributed throughout the nanofibers matrix, indicating a homogeneous loading of HKUST-1 within the PCL fibers. The EDS spectrum revealed that the nanofibers consisted of 66.38 wt% carbon, 30.28 wt% oxygen, and 0.51 wt% copper.

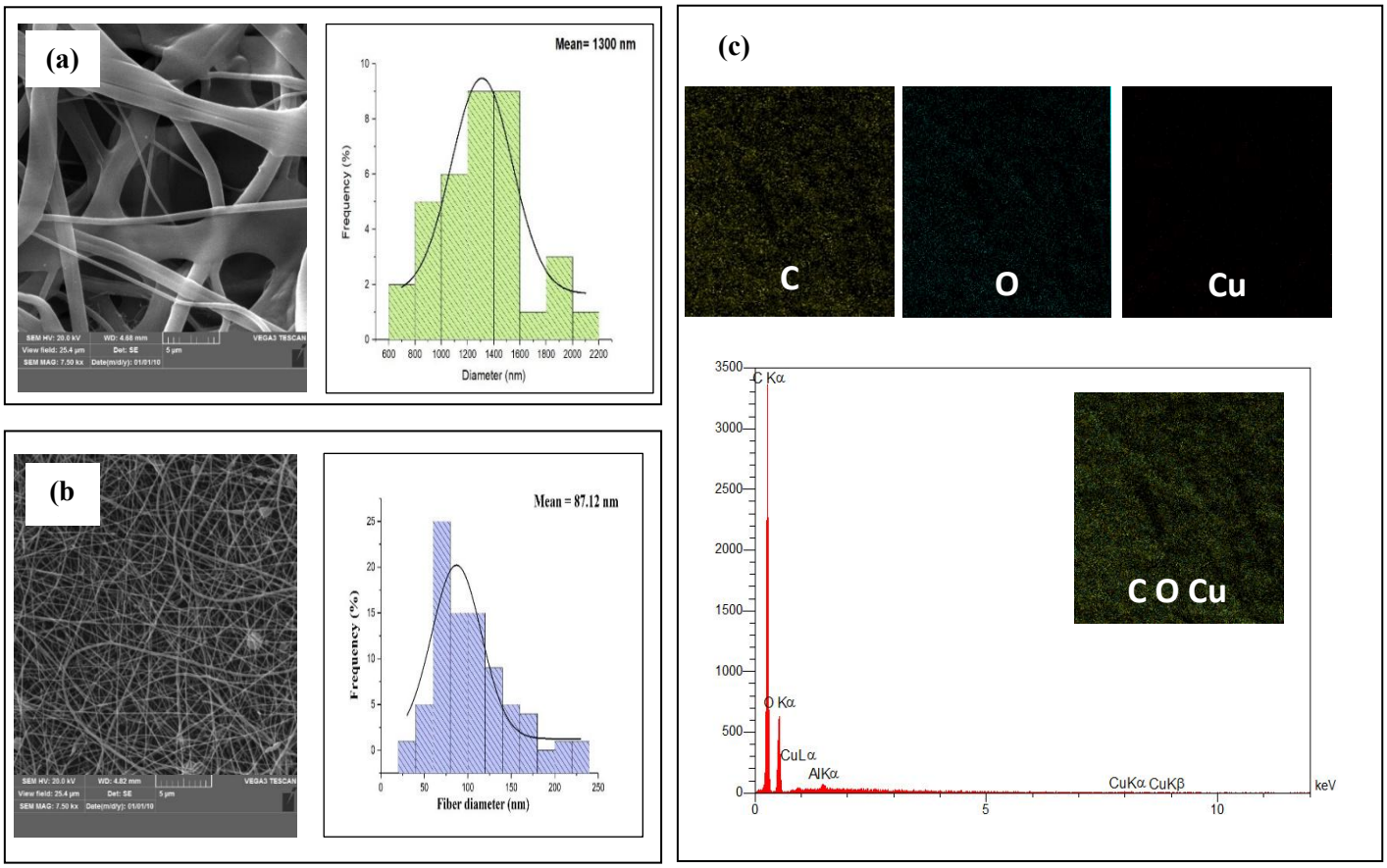


Fig. 6. Morphology analysis of the prepared fibers **(a)** SEM image and the Gaussian fiber diameter distribution of PF_1, **(b)** SEM image and the Gaussian fiber diameter distribution of NF_1-Cu and **(c)** SEM-EDS elemental mapping of NF_1-Cu

In addition, the SEM image and Gaussian fiber diameter distribution of the PCL/*Chlorella* polysaccharide nanofibers (ChNF) are reported in Fig. 7a. The results indicate that the addition of *Chlorella* polysaccharides to the PCL solution resulted in the formation of some beads along the fibers. The average diameter of the electrospun nanofibers was estimated to be 65.43 nm. SEM-EDS elemental mapping indicated the presence and distribution of carbon and oxygen on the nanofibers. The EDS analysis (Fig. 7b) revealed that the nanofibers contained 66.19 wt% carbon and 33.81 wt% oxygen.

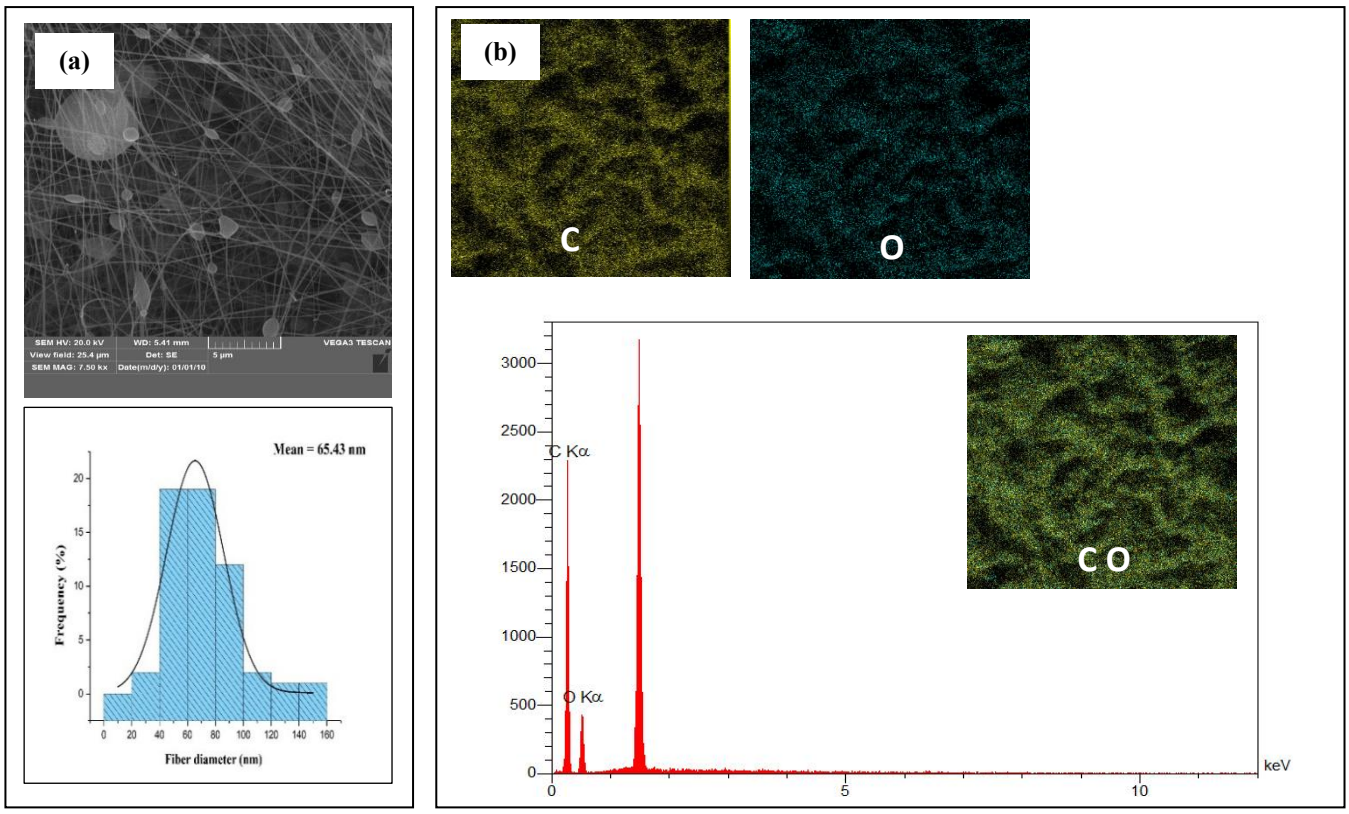


Fig. 7. Morphology analysis of the prepared PCL/*Chlorella* polysaccharide nanofibers (ChNF) **(a)** SEM image and the Gaussian fiber diameter distribution, and **(b)** SEM-EDS elemental mapping

The SEM images and Gaussian size distribution of the ChNC-Cu nanocomposites are presented in Fig. 8a. By adding the 4 wt% of HKUST-1 into the PCL-*Chlorella* polysaccharide solution, the mean dimater of the electrospun ChNC-Cu nanocomposite fibers increased to 125.33 nm while ChNC-Cu composites were aligned and smooth. As can be seen in SEM-EDS elemental mapping, the HKUST-1 nanoparticles were uniformly loaded on the nanocomposite without any beads (Fig. 8b). SEM-EDS elemental mapping results showed the presence of 3.96% copper by weight in the prepared nanofibers (Fig. 8b).

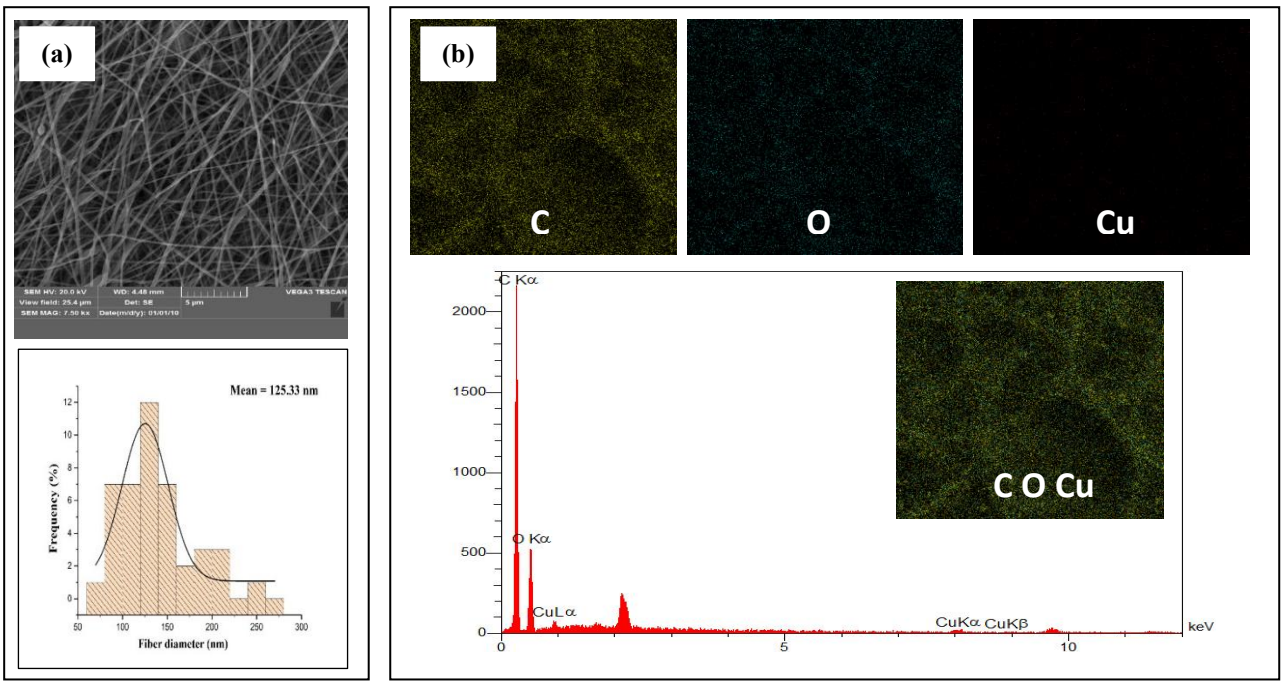


Fig. 8. Morphology analysis of prepared PCL/*Chlorella* polysaccharide/HKUST-1 nanocomposite (ChNC-Cu) **(a)** SEM image and the Gaussian fiber diameter distribution, and **(b)** SEM-EDS elemental mapping

In continuation, the SEM images of PCL/*Tetraselmis* polysaccharide nanofibers (TNF) are presented in Fig. 9a. The nanofibers exhibited a relatively uniform morphology, with the *Tetraselmis* polysaccharide particles distributed homogeneously throughout the PCL fibers. The mean diameter of the TNF nanofibers was estimated to be approximately 75 nm. According to the SEM-EDS elemental mapping results (Fig. 9b), the prominent carbon peak indicates a high carbon content in the sample, which is due to the presence of polycaprolactone as the main component of the nanofiber composition. The presence of oxygen, in addition to originating from polycaprolactone, may also be attributed to hydroxyl groups and other oxygen-containing groups within the structure of the *Tetraselmis* polysaccharide.

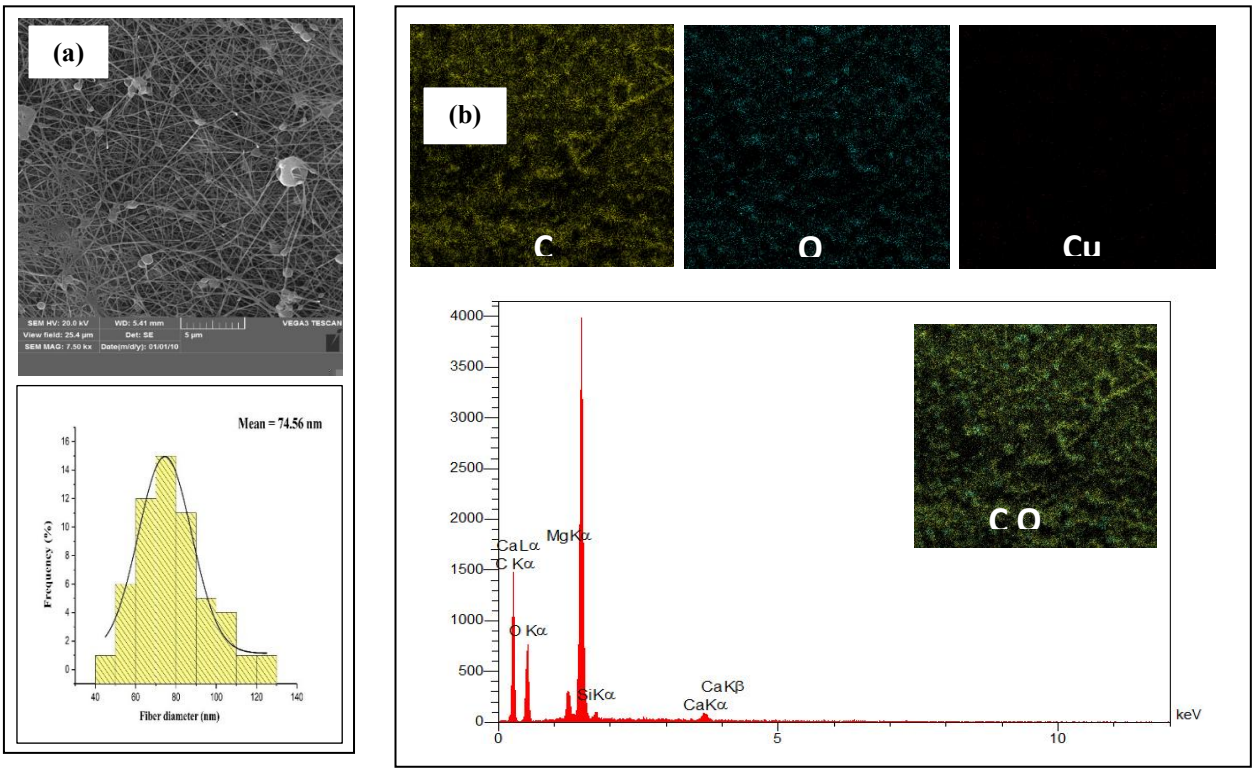


Fig. 9. Morphology analysis of prepared PCL/*Tetraselmis* polysaccharide nanofibers (TNF) **(a)** SEM image and the Gaussian distributions of TNF, and **(b)** SEM-EDS elemental mapping of TNF

Incorporating of 4 wt% of HKUST-1 into the the PCL/*Tetraselmis* polysaccharide solution resulted in an increase in the mean nanocomposite diameter to nearly 130 nm, with the composites exhibiting a smooth and aligned morphology (TNC-Cu) as can be seen in Fig. 10a. Additionally, the HKUST-1 nanoparticles were evenly distributed throughout the nanocomposite without forming any beads. SEM-EDS elemental mapping analysis, indicated controlled incorporation of copper into the nanofiber structure with a weight percentage of 2.71 (Fig. 10b).

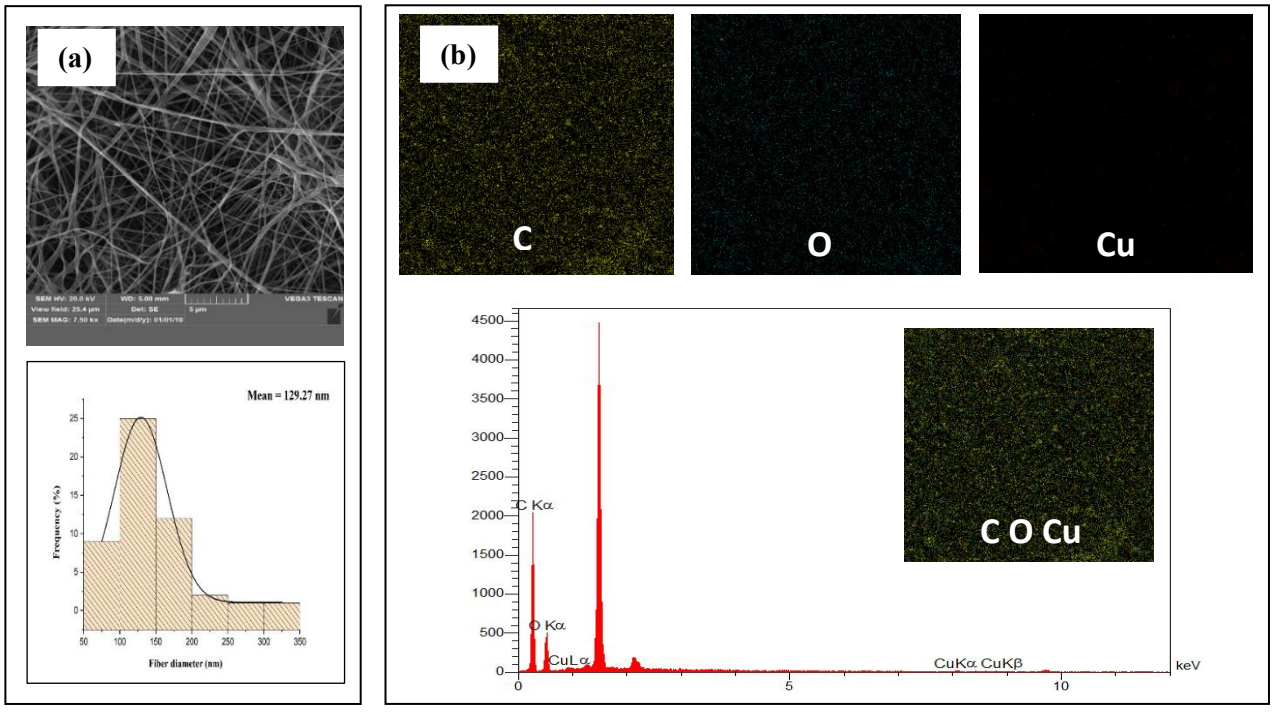


Fig. 10. Morphology analysis of prepared PCL/*Tetraselmis* polysaccharide/HKUST-1 nanocomposite (TNC-Cu) **(a)** SEM image and the Gaussian distributions of TNC-Cu, and **(b)** SEM-EDS elemental mapping of TNC-Cu

The results of adding HKUST-1 to the average diameters of the nanofibers are presented in Table 4. According to the reporting data, incorporation of HKUST-1 into PCL fibers drastically decreased the average diameter of the fibers. This behavior may be associated with changes in the electrical properties of the spinning solution induced by the addition of HKUST-1. In electrospinning process, an increase in the electrical conductivity of the solution can enhance charge accumulation on the polymer jet, resulting in greater electrostatic repulsion and enhanced jet stretching, which ultimately leads to the formation of the fibers with smaller diameters. However, adding HKUST-1 into ChNF and TNF nanofibers containing algal polysaccharides resulted in an increase in the average fiber diameters. This bahavior may be attributed to the complex intractions among PCL, HKUST-1, and algal polysaccharides. The addition of the polysaccharide can change the rheological and electrical properties of the spinning solution. An increase in viscosity can restrict jet deformation, thereby favoring the formation of fibers with larger diametes, whereas increased conductivity generally promotes thinner fibers [65, 66].

Table 4. The average diameters of the electrospun fibers

Nanofiber/ Nanocomposite names	**HKUST-1 to PCL ratio $(wt/wt)\%$**	**Mean fiber/composite diameter (nm)**
PF_1	0	1300
NF_1-Cu	4	87.12
ChNF	0	65.43
ChNC-Cu	4	125.33
TNF	0	74.56
TNC-Cu	4	129.27

3.2.3 Contact angle analysis

The relative hydrophobicity of the PCL/*Chlorella* polysaccharide (ChNF) and PCL/*Tetraselmis* polysaccharide (TNF) nanocomposites were determined by measuring the water contact angle. A water droplet was deposited on the surface of each nanocomposite, and the static water contact angle was measured within 1-2 seconds. Figs. 11 (a-f) show photographs of water droplets deposited on the surfaces of the electrospun nanocomposites. Adding *Chlorella* and *Tetraselmis* polysaccharides to PCL nanofibers,

the contact angle increased from 118° to 130° and 134°, respectively. These results indicate that the incorporation of the mentioned polysaccharides enhance the hydrophobicity of the PCL fibers. This increase in the water contact angle could be due to the low content of anionic or hydrophilic functional groups, such as sulfate and carboxyl groups, within the polysaccharide structures. Furthermore, the high molecular weight and compact structures of the polysaccharides may limit their effective exposure at the nanofiber surface during electrospinning, thereby resulting in poor wettability. In addition, the non-uniform dispersion of the polysaccharides could also result in a more hydrophobic surface with an increased contact angle.

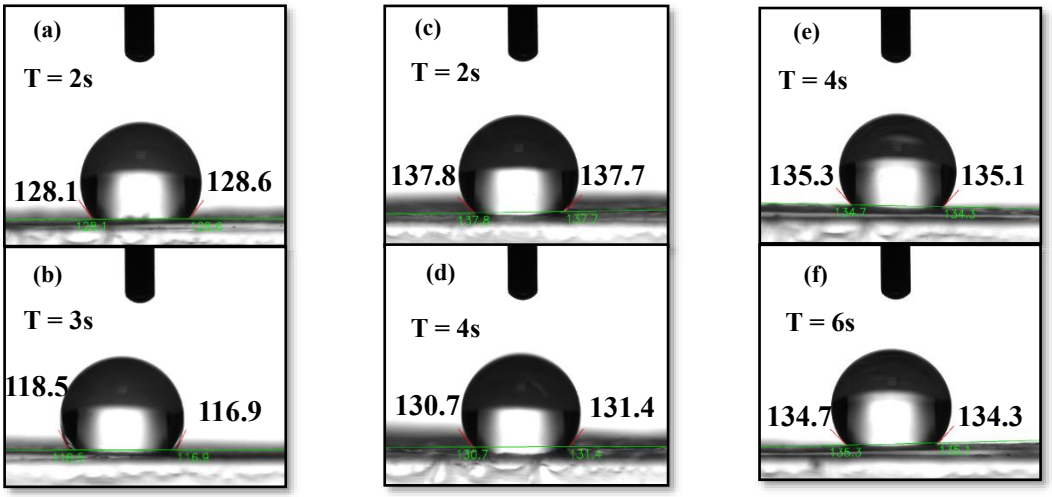


Fig. 11. Images of contact angle tests of **(a) & (b)** PCL fibers (PF1), **(c) & (d)** PCL/*Chlorella* polysaccharide nanocomposite (ChNF), and **(e) & (f)** PCL/*Tetraselmis* polysaccharide nanocomposite (TNF)

3. 3 Evaluation of Antibacterial Properties

3. 3. 1 Minimum Inhibitory Concentration (MIC) and Minimum Bactericidal Concentration (MBC)

The Minimum Inhibitory Concentration (MIC) is a test used to determine the lowest concentration of an antimicrobial agent that is needed to inhibit visible in-vitro growth of a challenge microorganism. The MBC refers to the minimum concentration of an antimicrobial agent that reduces the viability of the initial microorganism inoculation by ≥99.9%. The MIC test is often taken one step further to determine the Minimum Bactericidal Concentration (MBC) of agents [67, 68]. In this study to evaluate the antibacterial activity of the nanocomposites, MIC and MBC tests were performed against Staphylococcus aureus (*S. aureus*) and Escherichia coli (*E. coli*). These tests were performed with polysaccharide solutions from two algae; *Chlorella*, *Tetraselmis*, and a solution of HKUST-1. As presented in Table 5, the only tested sample that indicated clear

antibacterial activity against both strains were the copper-based MOF (HKUST-1) solution with MIC and MBC values of 3.75 and 7.5 mg/mL, respectively. The relatively small gap between these two values suggests that HKUST-1 acts bactericidally rather than merely bacteriostatically at slightly elevated concentrations. Algal polysaccharide solutions from *Chlorella* and *Tetraselmis* showed no inhibitory or bactericidal effect against *E. coli* at any tested concentration.

Table 5. MIC and MBC tests results of the samples on *E. coli*

Sample number	Sample	MBC (mg/ml)	MIC (mg/ml)
1	HKUST-1 solution	7.5	3.75
2	*Chlorella* Polysaccharide solution	-	-
3	*Tetraselmis* Polysaccharide solution	-	-

As shown in Table 6, against *S. aureus*, *Tetraselmis* polysaccharide showed a MIC of 25 mg/mL, a value roughly six times higher than that of HKUST-1, while no MBC could be determined within the tested range. No activity was recorded for *Chlorella* polysaccharide against either strain [69]. Based on the results, HKUST-1 has both bacteriostatic and bactericidal activities, and *Tetraselmis* polysaccharide shows selective bacteriostatic activity against Gram-positive bacteria.

Table. 6. MIC and MBC tests results of the samples on *S. aureus*

Sample number	Sample	MBC (mg/ml)	MIC (mg/ml)
1	HKUST-1 solution	7.5	3.75
2	*Chlorella* Polysaccharide solution	-	-
3	*Tetraselmis* Polysaccharide solution	-	25

3.1 DPPH test

The DPPH radical scavenging method is a common method used to assay the antioxidant activities of compounds from various sources. In this study to evaluate the antioxidant activity of the samples, a 1 mM solution of DPPH was mixed with the test samples at a ratio of 1:3 (v:v) and incubated in the dark at room temperature for 30 min. Subsequently, the absorbance was measured at 517 nm. Antioxidant test samples were introduced in syringes as solutions and considered at the highest concentration (x), which was diluted for further testing [70, 71]. The antioxidant activity of DPPH free radical scavenging was calculated by Eq (1) as follows:

$$\boldsymbol{Inhibition\ of\ DPPH}\ (\%) = \frac{\boldsymbol{Abs\ control - Abs\ sample}}{\boldsymbol{Abs\ control}} \times \mathbf{100} \qquad \text{Eq (1)}$$

Where Abs control is absorbance of the control and Abs sample is absorbance of the sample. According to results reported in Table 7, None of the tested samples exhibited

appreciable DPPH radical scavenging activity. Several concentrated samples produced absorbance values greater than the DPPH control, most likely due to interference from the intrinsic color of the samples rather than increased radical formation.

Table 7. The results of the antioxidant activity test of the samples using the DPPH method

Sample	The absorbance at concentration X	X/2	X/4	X/8	X/16
HKUST-1 solution	2.35	1.461	1.121	0.815	0.849
Chlorella solution	1.391	1.332	0.857	0.821	0.832
Tetraselmis solution	1.831	1.245	0.821	0.815	0.849

4. Conclusion

In this study, fibrous nanocomposites were fabricated via electrospinning using synthetic PCL and natural algal polysaccharides extracted from *Chlorella* and *Tetraselmis*. Owing to their poor chain entanglement, the algal polysaccharides alone were not readily electrospinnable. The incorporation of PCL enhanced the mechanical strength and solution viscosity, thereby enabling the formation of uniform nanofibers during electrospinning. HKUST-1, at an optimized loading of 4 wt% relative to PCL, was incorporated to improve antimicrobial properties of the nanocomposite. A three-layer PCL/algal polysaccharide/HKUST-1 nanocomposite was successfully developed as a structural platform with potential for biomedical applications. The choice of copper precursor was found to be an important parameter in HKUST-1 synthesis. Under identical synthetic conditions, the acetate-derived HKUST-1 exhibited higher crystallinity and a greater BET surface area than the nitrate-derived counterpart, highlighting the significant influence of the copper precursor on the structural properties of the resulting MOF. HKUST-1 addition reduced the average fiber diameter, while polysaccharide incorporation increased the fiber diameter to 125–130 nm in the final composites. Contact angle measurements further demonstrated that polysaccharide incorporation increased surface hydrophobicity, which was attributed to the compact molecular structure of the polysaccharides and their limited exposure at the fiber surface during electrospinning. Antibacterial evaluation of the HKUST-1 component demonstrated bactericidal activity against both *E. coli* and *S. aureus*, with MIC and MBC values of 3.75 and 7.5 mg/mL, respectively. In contrast, *Tetraselmis* polysaccharide exhibited selective bacteriostatic activity against *S. aureus*. However, whether the antibacterial activity of HKUST-1 is

retained following its incorporation into the fiber matrix and how copper ion release occurs under physiological conditions remain to be elucidated.

Acknowledgements

The authors thank the Alzahra Research Council for its partial financial support.

Author contributions

M. H.: Writing the main manuscript, Visualization, Validation, Methodology, Investigation, Conceptualization. Z. E. G.: Writing the main manuscript, Visualization, Validation, Investigation, Conceptualization.

References

[1] Heydari, P., Varshosaz, J., Zargar Kharazi, A., & Karbasi, S. (2018). Preparation and evaluation of poly glycerol sebacate/poly hydroxy butyrate core-shell electrospun nanofibers with sequentially release of ciprofloxacin and simvastatin in wound dressings. *Polymers for Advanced Technologies*, *29*(6), 1795–1803. https://doi.org/10.1002/pat.4286

[2] Zhao, J., Chen, L., Ma, A., Bai, X., Zeng, Y., Liu, D., Liu, B., Zhang, W., & Tang, S. (2024). Recent advances in coaxial electrospun nanofibers for wound healing. *Materials Today Bio*, *29*, 101309. https://doi.org/10.1016/j.mtbio.2024.101309

[3] Hasan, M. M., & Shahid, M. A. (2023). PVA, licorice, and collagen (PLC) based hybrid bio-nano scaffold for wound healing application. *Journal of Biomaterials Science, Polymer Edition*, *34*(9), 1217–1236. https://doi.org/10.1080/09205063.2022.2163454

[4] Ren, X., Hu, Y., Chang, L., Xu, S., Mei, X., & Chen, Z. (2022). Electrospinning of antibacterial and anti-inflammatory Ag@hesperidin core-shell nanoparticles into nanofibers used for promoting infected wound healing. *Regenerative Biomaterials*, *9*. https://doi.org/10.1093/rb/rbac012

[5] Tian, Y., Bao, X., Wang, S., Tang, C., Wu, N., Li, G., Ren, K., Yin, J., Yan, S., & Xu, G. (2025). A biomimetic nanofiber composite hydrogel with tissue adhesion, self-healing and antibacterial ability for infected wound healing. *Acta Biomaterialia*, *200*, 326–339. https://doi.org/10.1016/j.actbio.2025.04.002

[6] Wani, S., Sofi, H. S., Majeed, S., & Sheikh, F. A. (2017). Recent Trends in Chitosan Nanofibers: From Tissue-Engineering to Environmental Importance: A Review. *Material Science Research India*, *14*(2), 89–99. https://doi.org/10.13005/msri/140202

[7] Liu, H., Bai, Y., Huang, C., Wang, Y., Ji, Y., Du, Y., Xu, L., Yu, D.-G., & Bligh, S. W. A. (2023). Recent Progress of Electrospun Herbal Medicine Nanofibers. *Biomolecules*, *13*(1), 184. https://doi.org/10.3390/biom13010184

[8] Bhardwaj, N., & Kundu, S. C. (2010). Electrospinning: A fascinating fiber fabrication technique. *Biotechnology Advances*, *28*(3), 325–347. https://doi.org/10.1016/j.biotechadv.2010.01.004

[9] Coelho, S. A. R., Grenho, L., Fernandes, M. H. R., Fernandes, M. H. V., & Almeida, J. C. (2025). Organic–Inorganic Hybrid Nanofiber Membranes by Electrospinning: Engineering Features and Cytocompatibility. *ACS Applied Polymer Materials*, *7*(14), 9010–9024. https://doi.org/10.1021/acsapm.5c01072

[10] Haghighi, M., Taremi, F., Ghadim, Z.E. *et al.* Electrospun bi-layer carboxymethyl cellulose/polyvinyl alcohol/polycaprolactone nanofibers: fabrication, degradation, and phenytoin release kinetics. *Scientific Reports*, *16*, 16901 (2026). https://doi.org/10.1038/s41598-026-45707-7

[11] Badie, M. A., Teaima, M. H., El-Nabarawi, M. A., & Badawi, N. M. (2025). Novel hybrid nanofibers for burn wounds: Fucoidan-coated cefdinir nanoparticles in PVA matrices. *Journal of Drug Delivery Science and Technology*, *112*, 107184. https://doi.org/10.1016/j.jddst.2025.107184

[12] Lin, J., Jiao, G., & Kermanshahi-pour, A. (2022). Algal Polysaccharides-Based Hydrogels: Extraction, Synthesis, Characterization, and Applications. *Marine Drugs*, *20*(5), 306. https://doi.org/10.3390/md20050306

[13] Satchanska, G., Davidova, S., & Petrov, P. D. (2024). Natural and Synthetic Polymers for Biomedical and Environmental Applications. *Polymers*, *16*(8), 1159–1159. https://doi.org/10.3390/polym16081159

[14] Zheng, L., Zhu, Z., Pan, L., Zhong, L., Xiao, S., Zhao, C., Liu, Y., Xu, J., & Zhang, Y. (2025). Polysaccharides and proteins as natural polymers for electrospun wound dressings: A review of healing potential, challenges, and crosslinking strategies. *International Journal of Biological Macromolecules*, *320*, 145960. https://doi.org/10.1016/j.ijbiomac.2025.145960

[15] Doostmohammadi, M., Forootanfar, H., & Ramakrishna, S. (2020). Regenerative medicine and drug delivery: Progress via electrospun biomaterials. *Materials Science and Engineering: C*, *109*, 110521. https://doi.org/10.1016/j.msec.2019.110521

[16] Kumar, S., Marrero-Berrios, I., Kabat, M., & Berthiaume, F. (2019). Recent Advances in the Use of Algal Polysaccharides for Skin Wound Healing. *Current Pharmaceutical Design*, *25*(11), 1236–1248. https://doi.org/10.2174/1381612825666190521120051

[17] Pamshong, S. R., Murty, U. S., & Banerjee, S. (2025). Marine polysaccharides as promising 3D printable biomaterials for potential wound healing and antimicrobial therapeutics delivery: A review. *International Journal of Biological Macromolecules*, *322*, 147011. https://doi.org/10.1016/j.ijbiomac.2025.147011

[18] Huang, H., Lang, Y., & Zhou, M. (2024). A comprehensive review on medical applications of microalgae. *Algal Research*, 103504–103504. https://doi.org/10.1016/j.algal.2024.103504

[19] Lim, K. X., Wong, C. C., Sahu, M., Long, C. M., Nandave, M., & Yow, Y.-Y. (2026). Algal biomolecules and their potential applications in wound care and skin health: A systematic review. *Food Bioscience*, *80*, 109037. https://doi.org/10.1016/j.fbio.2026.109037

[20] El-Naggar, N. E.-A., Hussein, M. H., Shaaban-Dessuuki, S. A., & Dalal, S. R. (2020). Production, extraction and characterization of Chlorella vulgaris soluble polysaccharides and their applications in AgNPs biosynthesis and biostimulation of plant growth. *Scientific Reports*, *10*(1). https://doi.org/10.1038/s41598-020-59945-w

[21] Jo, W. S., Choi, Y. J., Kim, H. J., Nam, B. H., Hong, S. H., Lee, G. A., Lee, S. W., Seo, S. Y., & Jeong, M. H. (2010). Anti-inflammatory effect of microalgal extracts from Tetraselmis suecica. *Food Science and Biotechnology*, *19*(6), 1519–1528. https://doi.org/10.1007/s10068-010-0216-6

[22] Yu, M., Chen, M., Gui, J., Huang, S., Liu, Y., Shentu, H., He, J., Fang, Z., Wang, W., & Zhang, Y. (2019). Preparation of Chlorella vulgaris polysaccharides and their antioxidant activity in vitro and in vivo. *International Journal of Biological Macromolecules*, *137*, 139–150. https://doi.org/10.1016/j.ijbiomac.2019.06.222

[23] Capek, P., Matulová, M., Šutovská, M., Barboríková, J., Molitorisová, M., & Kazimierová, I. (2020). Chlorella vulgaris α-L-arabino-α-L-rhamno-α,β-D-galactan structure and mechanisms of its anti-inflammatory and anti-remodelling effects. *International Journal of Biological Macromolecules*, *162*, 188–198. https://doi.org/10.1016/j.ijbiomac.2020.06.151

[24] Amna Kashif, S., Hwang, Y. J., & Park, J. K. (2018). Potent biomedical applications of isolated polysaccharides from marine microalgae Tetraselmis species.

Bioprocess and Biosystems Engineering, *41*(11), 1611–1620. https://doi.org/10.1007/s00449-018-1987-z

[25] Gobi, R., Ravichandiran, P., Babu, R. S., & Yoo, D. J. (2021). Biopolymer and Synthetic Polymer-Based Nanocomposites in Wound Dressing Applications: A Review. *Polymers*, *13*(12), 1962. https://doi.org/10.3390/polym13121962

[26] Naveen Palani, Vijayakumar, P., P. Monisha, Saravanakumar Ayyadurai, & Suriyaprakash Rajadesingu. (2024). Electrospun nanofibers synthesized from polymers incorporated with bioactive compounds for wound healing. *Journal of Nanobiotechnology*, *22*(1). https://doi.org/10.1186/s12951-024-02491-8

[27] Ntrivala, M. A., Pitsavas, A. C., Lazaridou, K., Baziakou, Z., Karavasili, D., Papadimitriou, M., Ntagkopoulou, C., Balla, E., & Bikiaris, D. N. (2025). Polycaprolactone (PCL): the biodegradable polyester shaping the future of materials – a review on synthesis, properties, biodegradation, applications and future perspectives. *European Polymer Journal*, *234*, 114033. https://doi.org/10.1016/j.eurpolymj.2025.114033

[28] Woodruff, M. A., & Hutmacher, D. W. (2010). The return of a forgotten polymer—Polycaprolactone in the 21st century. *Progress in polymer science*, *35*(10), 1217-1256. https://doi.org/10.1016/j.progpolymsci.2010.04.002

[29] Rajabifar, N., Rostami, A., Afshar, S., Mosallanezhad, P., Zarrintaj, P., Shahrousvand, M., & Nazockdast, H. (2024). Wound Dressing with Electrospun Core-Shell Nanofibers: From Material Selection to Synthesis. *Polymers*, *16*(17), 2526. https://doi.org/10.3390/polym16172526

[30] Musciacchio, L., Mardirossian, M., Marussi, G., Crosera, M., Turco, G., & Porrelli, D. (2025). Core-shell electrospun polycaprolactone nanofibers, loaded with rifampicin and coated with silver nanoparticles, for tissue engineering applications. *Biomaterials Advances*, *166*, 214036. https://doi.org/10.1016/j.bioadv.2024.214036.

[31] Oliveira, C., Sousa, D., Teixeira, J. A., Ferreira-Santos, P., & Botelho, C. M. (2023). Polymeric biomaterials for wound healing. *Frontiers in Bioengineering and Biotechnology*, *11*, 1136077. https://doi.org/10.3389/fbioe.2023.1136077

[32] Aderibigbe, B. A. (2022). Hybrid-Based Wound Dressings: Combination of Synthetic and Biopolymers. *Polymers*, *14*(18), 3806. https://doi.org/10.3390/polym14183806

[33] Gul, A., Gallus, I., Tegginamath, A., Maryska, J., & Yalcinkaya, F. (2021). Electrospun Antibacterial Nanomaterials for Wound Dressings Applications. *Membranes*, *11*(12), 908. https://doi.org/10.3390/membranes11120908

[34] Zhao, J., Chen, L., Ma, A., Bai, X., Zeng, Y., Liu, D., Liu, B., Zhang, W., & Tang, S. (2024). Recent advances in coaxial electrospun nanofibers for wound healing. *Materials Today Bio*, *29*, 101309. https://doi.org/10.1016/j.mtbio.2024.101309

[35] Gautam, S., Lakhanpal, I., Sonowal, L., & Goyal, N. (2023). Recent advances in targeted drug delivery using metal-organic frameworks: toxicity and release kinetics. *Next Nanotechnology*, *3–4*, 100027. https://doi.org/10.1016/j.nxnano.2023.100027

[36] Lawson, H. D., Walton, S. P., & Chan, C. (2021). Metal–Organic Frameworks for Drug Delivery: A Design Perspective. *ACS Applied Materials & Interfaces*, *13*(6), 7004–7020. https://doi.org/10.1021/acsami.1c01089

[37] Cun, J.-E., Fan, X., Pan, Q., Gao, W., Luo, K., He, B., & Pu, Y. (2022). Copper-based metal–organic frameworks for biomedical applications. *Advances in Colloid and Interface Science*, *305*, 102686. https://doi.org/10.1016/j.cis.2022.102686

[38] Gulia, M., & Thakur, A. (2025). Copper-based metal–organic framework (Cu-MOF) as a cost-effective antimicrobial and antioxidant reagent: synthesis, characterization and biological evaluation. *Chemical Papers*, *79*(7), 4317–4329. https://doi.org/10.1007/s11696-025-04058-9

[39] Zhong, J., Kankala, R. K., Wang, S.-B., & Chen, A.-Z. (2019). Recent Advances in Polymeric Nanocomposites of Metal-Organic Frameworks (MOFs). *Polymers*, *11*(10), 1627. https://doi.org/10.3390/polym11101627

[40] Michaleas, S. N., Laios, K., Charalabopoulos, A., Samonis, G., & Karamanou, M. (2022). Joseph Lister (1827-1912): A Pioneer of Antiseptic Surgery. *Cureus*, *14*(12). https://doi.org/10.7759/cureus.32777

[41] Jones, J. (2005). Winter's concept of moist wound healing: a review of the evidence and impact on clinical practice. *Journal of Wound Care*, *14*(6), 273–276. https://doi.org/10.12968/jowc.2005.14.6.26794

[42] Kumar, S. P., Asokan, Y., Balamurugan, K., & Harsha, B. (2022). A review of wound dressing materials and its fabrication methods: emphasis on three-dimensional printed dressings. *Journal of Medical Engineering & Technology*, *46*(4), 318–334. https://doi.org/10.1080/03091902.2022.2041750

[43] Kikionis, S., Ioannou, E., Toskas, G., & Roussis, V. (2015). Electrospun biocomposite nanofibers of ulvan/PCL and ulvan/PEO. *Journal of Applied Polymer Science*, *132*(26). https://doi.org/10.1002/app.42153

[44] Jung, S. M., Min, S. K., Lee, H. C., Kwon, Y. S., Jung, M. H., & Shin, H. S. (2016). Spirulina-PCL nanofiber wound dressing to improve cutaneous wound healing by enhancing antioxidative mechanism. *Journal of nanomaterials*, *2016*(1), 6135727. https://doi.org/10.1155/2016/6135727

[45] Choi, J. I., Kim, M. S., Chung, G. Y., & Shin, H. S. (2017). Spirulina extract-impregnated alginate-PCL nanofiber wound dressing for skin regeneration. *Biotechnology and Bioprocess Engineering*, *22*(6), 679-685. https://doi.org/10.1007/s12257-017-0329-3

[46] Shi, R., Geng, H., Gong, M., Ye, J., Wu, C., Hu, X., & Zhang, L. (2018). Long-acting and broad-spectrum antimicrobial electrospun poly (ε-caprolactone)/gelatin micro/nanofibers for wound dressing. *Journal of colloid and interface science*, *509*, 275-284. https://doi.org/10.1016/j.jcis.2017.08.092

[47] Ghaee, A., Bagheri-Khoulenjani, S., Amir Afshar, H., & Bogheiri, H. (2019). Biomimetic nanocomposite scaffolds based on surface modified PCL-nanofibers containing curcumin embedded in chitosan/gelatin for skin regeneration. *Composites Part B: Engineering*, *177*, 107339. https://doi.org/10.1016/j.compositesb.2019.107339

[48] Dodero, A., Alloisio, M., Castellano, M., & Vicini, S. (2020). Multilayer Alginate–Polycaprolactone Electrospun Membranes as Skin Wound Patches with Drug Delivery Abilities. *ACS Applied Materials & Interfaces*, *12*(28), 31162–31171. https://doi.org/10.1021/acsami.0c07352

[49] Abou-Okeil, A., Fahmy, H. M., Fouda, M. M. G., Aly, A. A., & Ibrahim, H. M. (2021). Hyaluronic Acid/Oxidized Κ-Carrageenan Electrospun Nanofibers Synthesis and Antibacterial Properties. *BioNanoScience*, *11*(3), 687–695. https://doi.org/10.1007/s12668-021-00884-9

[50] Zulema Vargas Osorio, Florian Florian Ruther, Chen, S., Sengupta, S., Liverani, L., Michálek, M., Dušan Galusek, & Boccaccini, A. R. (2022). Environmentally friendly fabrication of electrospun nanofibers made of polycaprolactone, chitosan and κ-carrageenan (PCL/CS/κ-C). *Biomedical Materials*, *17*(4), 045019–045019. https://doi.org/10.1088/1748-605x/ac6eaa

[51] Fahimirad, S., Satei, P., Ganji, A., & Abtahi, H. (2022). Wound healing performance of PVA/PCL based electrospun nanofiber incorporated green synthetized

CuNPs and *Quercus infectoria* extracts. *Journal of Biomaterials Science, Polymer Edition*, *34*(3), 277–301. https://doi.org/10.1080/09205063.2022.2116209

[52] Norouzi, M. R., Ghasemi-Mobarakeh, L., Itel, F., Schoeller, J., Fashandi, H., Fortunato, G., & Rossi, R. M. (2024). Dual Functional Antibacterial-Antioxidant Core/Shell Alginate/Poly(ε-caprolactone) Nanofiber Membrane: A Potential Wound Dressing. *ACS omega*, *9*(23), 25124–25134. https://doi.org/10.1021/acsomega.4c02510

[53] Kenawy, E.-R., Kamoun, E. A., Shehata, A., El-Moslamy, S. H., & Abdel-Rahman, A. A.-H. (2025). Biosynthesized ZnO NPs loaded-electrospun PVA/sodium alginate/glycine nanofibers: synthesis, spinning optimization and antimicrobial activity evaluation. *Scientific Reports*, *15*(1). https://doi.org/10.1038/s41598-024-81939-1

[54] Ali Hussein, R., Mohamed Abdo, S., Mahmoud, K., Mohamed Youssef, E., & Hussein Ali Ahmed, G. (2026). Microalgae-derived polyhydroxyalkanoate/PCL composite nanofiber scaffolds for accelerated wound healing in diabetic rats. *Journal of biomaterials science. Polymer edition*, 1–19. Advance online publication. https://doi.org/10.1080/09205063.2026.2684335*Edition*, 1–19. https://doi.org/10.1080/09205063.2026.2684335

[55] Guerrero, V. V., Yoo, Y., McCarthy, M. C., & Jeong, H.-K. (2010). HKUST-1 membranes on porous supports using secondary growth. *Journal of Materials Chemistry* (Vol. 20, Issue 19, p. 3938). https://doi.org/10.1039/b924536g

[56] Luo, Y., Chen, D., Wei, F., & Liang, Z. (2018). Synthesis of Cu-BTC metal-organic framework by ultrasonic wave-assisted ball milling with enhanced congo red removal property. *ChemistrySelect*, *3*(41), 11435-11440. https://doi.org/10.1002/slct.201802067

[57] Huang, W., Chen, Y., Hu, J., Yao, W., You, L., & Cheung, P. C.-K. (2022). Algal sulfated polysaccharide-based hydrogels enhance gelling properties and in vitro wound healing compared to conventional hydrogels. *Algal Research* (Vol. 65, p. 102740). https://doi.org/10.1016/j.algal.2022.102740

[58] Pan, H., Fan, D., Zhu, C., Duan, Z., Fu, R., & Li, X. (2019). Preparation of physically crosslinked PVA/HLC/SA hydrogel and exploration of its effects on full-thickness skin defects. *International Journal of Polymeric Materials and Polymeric Biomaterials*, *68*(17), 1048–1057. https://doi.org/10.1080/00914037.2018.1525547

[59] McInnes, S., Macdonald, T., Parkin, I., Nann, T., & Voelcker, N. (2018). Electrospun Composites of Polycaprolactone and Porous Silicon Nanoparticles for the

Tunable Delivery of Small Therapeutic Molecules. *Nanomaterials*, *8*(4), 205. https://doi.org/10.3390/nano8040205

[60] Liu, Q., Gao, Y., Zhou, Y., Tian, N., Liang, G., Ma, N., & Dai, W. (2019). Highly Improved Water Resistance and Congo Red Uptake Capacity with a Zn/Cu-BTC@MC Composite Adsorbent. *Journal of Chemical & Engineering Data*, *64*(8), 3323–3330. https://doi.org/10.1021/acs.jced.9b00159

[61] Md Zainul Abedeen, Harshita Laddha, Sharma, M., Gupta, R., & Himmat Singh Kushwaha. (2023). Non-enzyme picomolar sensing of acephate by modified glassy carbon electrode using bimetallic Zn-Cu metal-organic framework. *Journal of Electroanalytical Chemistry*, *948*, 117810–117810. https://doi.org/10.1016/j.jelechem.2023.117810

[62] Dai, W., Tian, N., Liu, C., Yu, Le, Liu, Q., Ma, N., & Zhao, Y. (2017). (Zn, Ni, Cu)-BTC Functionalized with Phosphotungstic Acid for Adsorptive Desulfurization in the Presence of Benzene and Ketone. *Energy & Fuels*, *31*(12), 13502–13508. https://doi.org/10.1021/acs.energyfuels.7b02851

[63] Minh, T. T., Tu, N. T. T., Van Thi, T. T., Hoa, Le T., Long, H. T., Phong, N. H., Pham, T. Le M., & Khieu, D. Q. (2019). Synthesis of Porous Octahedral ZnO/CuO Composites from Zn/Cu-Based MOF-199 and Their Applications in Visible-Light-Driven Photocatalytic Degradation of Dyes. *Journal of Nanomaterials*, *2019*, 1–16. https://doi.org/10.1155/2019/5198045

[64] Mokrzycki, J., Wolak, E., Orzechowska-Zieba, A., Zheng, K., Duraczyńska, D., Marzec, M., & Fedyna, M. (2024). The effect of copper(II) salt precursor on physicochemical properties of HKUST-1 MOFs and their application as adsorbents of Cr(III) ions from aqueous solutions. *Journal of Water Process Engineering*, *64*, 105761. https://doi.org/10.1016/j.jwpe.2024.105761

[65] Kim, J. W., Park, S., Park, K., & Kim, B.-K. (2023). Non-Toxic Natural Additives to Improve the Electrical Conductivity and Viscosity of Polycaprolactone for Melt Electrospinning. *Applied Sciences*, *13*(3), 1844. https://doi.org/10.3390/app13031844

[66] Shaban, M., Mosa, T.M., Abdel-Hamid, H. *et al.* Advancements in electrospinning: a comprehensive review of historical development, key parameters, applications, and challenges. *Discov. Chem.* **3**, 82 (2026). https://doi.org/10.1007/s44371-026-00539-2

[67] Azad, F. N., Ghaedi, M., Dashtian, K., Hajati, S., & Pezeshkpour, V. (2016). Ultrasonically assisted hydrothermal synthesis of activated carbon–HKUST-1-MOF hybrid for efficient simultaneous ultrasound-assisted removal of ternary organic dyes and antibacterial investigation: Taguchi optimization. *Ultrasonics Sonochemistry*, *31*, 383–393. https://doi.org/10.1016/j.ultsonch.2016.01.024

[68] Parvekar, P., Palaskar, J., Metgud, S., Maria, R., & Dutta, S. (2020). The minimum inhibitory concentration (MIC) and minimum bactericidal concentration (MBC) of silver nanoparticles against Staphylococcus aureus. *Biomaterial Investigations in Dentistry*, *7*(1), 105–109. https://doi.org/10.1080/26415275.2020.1796674

[69] Balouiri, M., Sadiki, M., & Ibnsouda, S. K. (2016). Methods for in vitro evaluating antimicrobial activity: a review. *Journal of Pharmaceutical Analysis*, *6*(2), 71–79. https://doi.org/https://doi.org/10.1016/j.jpha.2015.11.005

[70] Sharma, V., & Agarwal, A. (2015). Physicochemical and antioxidant assays of methanol and hydromethanol extract of ariel parts of Indigofera tinctoria Linn. *Indian Journal of Pharmaceutical Sciences*, *77*(6), 729. https://doi.org/10.4103/0250-474x.174995

[71] Sarker, S. D. (2004). Free radical scavenging activity of some Bangladeshi plant extracts. *Oriental Pharmacy and Experimental Medicine*, *4*(3), 187-195. https://doi.org/10.3742/opem.2004.4.3.187